

Nonlocal orientational distribution of contact forces in granular samples containing elongated particles

H. Magoaric · A. Danescu · B. Cambou

Received: 23 March 2007 / Accepted: 25 November 2007 / Published online: 22 February 2008
© Springer-Verlag 2008

Abstract In this paper we introduce the branch tensor as an internal variable able to account for the structural anisotropy of a granular sample. The distribution of averaged contact forces is assumed to depend not only on the macroscopic stress and the local orientation, but also on the value of the fabric tensor. In contrast to previous work, including the fabric tensor has the crucial advantage that accounts for all relative positions between interacting particles, through the average value of the branch tensor. Based on a classical representation result, we propose an identification procedure that uses information obtained from both isotropic and anisotropic configurations.

Keywords Anisotropic granular materials · Contact forces distribution · Fabric tensor · Localization

1 Introduction

Despite simple physical laws governing the micro-scale response, granular materials exhibit a complex behavior at the macroscopic level. Among the well-known characteristics of granular assemblies are the dilatancy and the irreversible evolution of micro-structure. The theoretical framework designed to relate description from the microscopic level to that of the macroscopic one is the homogenization theory. It is well accepted that relations between local interaction forces and macroscopic stress are

easy to obtain at any scale through the Weber relation. The reverse path, i.e., localization of the macroscopic stress, is a much more complicated procedure and a definite relation for the representation of averaged contact forces is not yet available.

Numerical tests performed on granular samples consisting of elongated particles [11] reveal that the orientational distribution of contact forces does not follow a similar evolution to that of samples with spherical and nearly spherical particles. One conclusion is that some additional internal variables had to be accounted for in order to include in the localization operator a structural part of the sample. The simplest choice in this direction is provided by the average over the sample of the contact tensor $\mathbf{C} = \langle \mathbf{n} \otimes \mathbf{n} \rangle$ [9, 12]. Following this line, we found in [2] that the evolution of the contact tensor is relatively weak. A possible explanation is that \mathbf{C} does not include enough information about the relative positions of neighboring particles but only information on the contacts themselves.

The use of fabric tensor-dependent material parameters falls into a larger class of models called materials with microstructure. Among the fruitful attempts to extend classical elastoplasticity in order to include the effects of the packing structure we cite [3, 7, 10]. The distribution of contact forces in terms of macroscopic stress was studied in [6] who noted a strong dependence of the probability distribution function on the contact orientation and consequently uses conditional probability distribution function in order to include the relation between the macroscopic stress and contact forces (relation (8) in this paper) in the analysis. We adopt here a different point of view and restrict only to analytical relations between orientational averaged contact forces and macroscopic stress that satisfy a priori (8) but include the averaged branch tensor. Its role

H. Magoaric (✉) · A. Danescu · B. Cambou
LTDS - UMR 5513,
Ecole Centrale de Lyon,
69134 Ecully, France
e-mail: helene.magoaric@ec-lyon.fr

in the present context is twofold: it reflects the packing structure and enlarges the class of admissible contact force distribution shapes to cover more than previously proposed elliptic shapes [5].

This paper introduces in the localization procedure the branch tensor defined as $\mathbf{H} = \langle \mathbf{l} \otimes \mathbf{l} \rangle$. This particular choice has some physical justifications. First, the branch vector \mathbf{l} measures the relative positions of particles including in a certain sense the microstructure of the sample. Secondly, in the particular case when explicit formulae are available in classical homogenization theory, they show that interaction forces between particles do actually depend on all relative positions of particles in the sample. The special case of elongated particles is of particular interest since structural anisotropy manifests strongly even in simple biaxial tests.

This paper is organized as follows: for completeness, Sect. 2 recalls the basic relations between the local interaction forces and macroscopic stress. The three variants of Weber relation are well-known, but they underline the specific role of the branch tensor as a choice for the description of the local structure of the granular sample. Section 3 states the basic representation result used in the following to identify the orientational distribution of contact forces. For the interested reader and since the representation result is purely technical, we choose to sketch the proof in an appendix. Section 4 presents the characteristics of the numerical samples we used. Section 5 describes the identification procedure which distinguishes between material parameters associated to the isotropic part of the representation, and thus identified on the most isotropic configuration, and the ones associated to the anisotropic part and identified on the most anisotropic configuration. The best way to figure this choice is a parallel to classical models of elastoplasticity in which case the elastic characteristics are identified using data within elastic range while plastic characteristics, such as hardening, are identified using data from the plastic regime. Finally, we compare our predictions with distributions obtained from numerical computations and discuss the predictive character of our result. We conclude the paper with comments and some open questions.

2 Contact forces and macroscopic stress

2.1 Weber relation

Consider a collection of granular particles \mathcal{P} at static equilibrium and denote by $\{\mathbf{F}^i\}_{i=1\dots M}$ the external forces acting on its boundary $\partial\mathcal{P}$. A well-known relation, called the *Weber formula*, defines the macroscopic stress as

$$\Sigma = \frac{1}{|\mathcal{P}|} \sum_{i=1}^M \mathbf{F}^i \otimes \mathbf{O}\mathbf{P}^i. \quad (1)$$

Here \mathbf{O} is an arbitrary point and \mathbf{P}^i are points on the boundary $\partial\mathcal{P}$ where \mathbf{F}^i acts. Relation (1) shows that the macroscopic stress depends only on the forces acting on the boundary $\partial\mathcal{P}$. Using equilibrium for each individual particle, the Weber relation can be also expressed:

- Using all forces acting on all particles in the granular sample as

$$\Sigma = \frac{1}{|\mathcal{P}|} \sum_{\mathcal{P}_i \in \mathcal{P}} \mathbf{F}^{ji} \otimes \mathbf{O}_i \mathbf{P}^{ji} \quad (2)$$

where \mathbf{F}^{ji} denotes the force acting from particle¹ \mathcal{P}_j on particle \mathcal{P}_i at common contact point \mathbf{P}^{ji} , and \mathbf{O}_i denotes the center of mass of particle \mathcal{P}_i .

- Using the vectors joining the centers of two particles in contact, usually called *branch vectors*, as

$$\Sigma = \frac{1}{|\mathcal{P}|} \sum_{(i,j)} \mathbf{F}^{ji} \otimes \mathbf{O}_i \mathbf{O}_j + \frac{1}{|\mathcal{P}|} \sum_{i=1}^M \mathbf{F}^i \otimes \mathbf{O}_j \mathbf{P}^{ji}. \quad (3)$$

The second term above contains all external forces \mathbf{F}^i acting on a particle \mathcal{P}_j , and $\mathbf{O}_j \mathbf{P}^{ji}$ denotes the vector joining \mathbf{O}_j —the center of mass of particle \mathcal{P}_j —to the point \mathbf{P}^{ji} where \mathbf{F}^i acts.

It was proved by Caillerie [1] that under suitable uniformity assumptions the second term in (3) is much smaller than the first one so that

$$\Sigma \simeq \frac{1}{|\mathcal{P}|} \sum_{(i,j)} \mathbf{F}^{ji} \otimes \mathbf{l}_{ij}, \quad (4)$$

where \mathbf{l}_{ij} denotes the branch vector $\mathbf{O}_i \mathbf{O}_j$.

2.2 Orientational distribution

If we rewrite the right-hand-side in (4) by sorting the contacts under ascendent orientation, we obtain

$$\sum_{(i,j)} \mathbf{F}^{ji} \otimes \mathbf{l}_{ij} = \sum_{\theta \uparrow} \mathbf{F}^{ji} \otimes \mathbf{l}_{ij}. \quad (5)$$

At a fixed orientational resolution $k \in \mathbb{N}^*$, we replace the individual values of the tensor product above by the average value computed over all contacts with orientation $\mathbf{n}(\theta)$ for θ in an interval of length $2\pi/k$. If N denotes the total number of contacts and N_a the number of contacts with normal oriented by θ in the interval $[2\pi(a-1)/k, 2\pi a/k]$, we have

¹ In this sum external forces should also be accounted for.

$$\sum_{\theta \uparrow} \mathbf{F}^{ji} \otimes \mathbf{l}_{ij} = N \sum_{a=1}^k \frac{N_a}{N} \langle \mathbf{F}^{ij} \otimes \mathbf{l}_{ij} \rangle_a. \tag{6}$$

For the next step we check numerically that forces and branch vectors are *noncorrelated* in which case

$$\boldsymbol{\Sigma} = \frac{N}{|\mathcal{P}|} \sum_{a=1}^k \frac{N_a}{N} \langle \mathbf{F}^{ij} \rangle_a \otimes \langle \mathbf{l}_{ij} \rangle_a \tag{7}$$

The continuum limit of the right-hand-side above is

$$\boldsymbol{\Sigma} = \frac{N\bar{d}}{|\mathcal{P}|} \int_0^{2\pi} p(\theta) \mathbf{f}(\boldsymbol{\Sigma}, \mathbf{n}) \otimes \mathbf{n} d\theta \tag{8}$$

where \bar{d} denotes a *characteristic length*. To deduce (8) from (7) we need an additional assumption about the orientational average of the branch vector, which is $\langle \mathbf{l} \rangle_a = \bar{d}\mathbf{n}$. Previous work on stress localization [4, 8, 11], consider \bar{d} as the averaged particles diameter, choice reconsidered hereafter.

The physical meaning of relation (8) is the following: given a macroscopic stress $\boldsymbol{\Sigma}$ among all admissible contact forces distributions only those satisfying (2) may appear in a granular assembly. From a statistical point of view, when detailed information about the local arrangement is not available, the orientational averaged contact forces and the macroscopic stress may still be related through (8) and this restricts the class of analytical relations between the contact force distribution and the macroscopic stress.

If we introduce a characteristic length $\bar{l} = |\mathcal{P}|/(\pi N\bar{d})$ and if we denote by \mathbf{f} the mean contact forces weighted by $p(\theta)$, relation (8) is identically satisfied by the one-parameter relation [5, 13]

$$\mathbf{f} = \bar{l} \left[\frac{1}{2} \text{tr} \boldsymbol{\Sigma} \mathbf{n} + 2(1 - \mu)(\mathbf{n} \cdot (\text{dev} \boldsymbol{\Sigma}) \mathbf{n}) \mathbf{n} + \mu(\text{dev} \boldsymbol{\Sigma}) \mathbf{n} \right]. \tag{9}$$

It is straightforward to check that this relation leads to an ellipsoidal orientational distribution for the contact forces, well-fitted by numerical results for samples containing particles with aspect ratio² close to unity.

The situation is more complicated for samples containing elongated particles. Numerical results obtained with the Contact Dynamics software for polygonal particles with an aspect ratio of 3, show that relation (9) may not be sufficient and one simple way to circumvent this difficulty is to introduce an internal variable able to account for the microstructure of the sample. In support to this idea we note the following three arguments:

- (1) The work reported in [2] uses the average contact tensor $\mathbf{C} = \langle \mathbf{n} \otimes \mathbf{n} \rangle$; this choice was guided by earlier use of the contact tensor in the representation of the weighted contact forces [5, 8]. In this way the representation relation is enriched and we fit better the numerical data but still the anisotropy captured by the contact tensor evolves slowly.
- (2) Classical work in homogenization theory for elastic interactions [14] provides a localization relation which formally is identical to (1) but where the values of pairwise interactions depend not only on the local material structure but also on all other relative positions. In the actual setting this remark suggests the use of the branch tensor instead of contact tensor.
- (3) We note that contact orientations do not contain any particular information on the relative positions of particles in contact, except in the very special case of spherical particles. By inspection in (4) one may note that the macroscopic stress depends on the contact forces and relative positions but not on the contacts orientations, so that it seems more natural to include in the localization operator the branch tensor instead of the contact tensor.

Based on the above arguments, in the following we shall assume that the orientational distribution of contact forces is a function of the macroscopic stress $\boldsymbol{\Sigma}$, the local orientation \mathbf{n} and the average branch tensor $\langle \mathbf{l}^{ji} \otimes \mathbf{l}^{ji} \rangle$, subsequently denoted \mathbf{H} .

3 Representation result for weighted contact forces

Note that by definition the branch tensor \mathbf{H} is symmetric and $\mathbf{f}(\boldsymbol{\Sigma}, \mathbf{H}, \mathbf{n})$ has to satisfy

- (R1) **The consistency relation (8):** for any symmetric tensors $\boldsymbol{\Sigma}$ and \mathbf{H}

$$\boldsymbol{\Sigma} = \frac{1}{l\pi} \int_0^{2\pi} \mathbf{f}(\boldsymbol{\Sigma}, \mathbf{H}, \mathbf{n}) \otimes \mathbf{n} d\theta. \tag{10}$$

- (R2) **The frame-indifference assumption:** for any orthogonal transformation \mathbf{Q} and any symmetric tensors $\boldsymbol{\Sigma}$ and \mathbf{H}

$$\mathbf{f}(\mathbf{Q}\boldsymbol{\Sigma}\mathbf{Q}^t, \mathbf{Q}\mathbf{H}\mathbf{Q}^t, \mathbf{Q}\mathbf{n}) = \mathbf{Q}\mathbf{f}(\boldsymbol{\Sigma}, \mathbf{H}, \mathbf{n}). \tag{11}$$

Usually, the local contact forces are assumed to be linear with respect to $\boldsymbol{\Sigma}$ and no more than affine with respect to \mathbf{H} .

A long but straightforward calculation using classical methods in representation theory³ shows that in the two-dimensional case: the most general form of a function

² We use aspect ratio to denote $\max_{\phi} (\text{diam}(\phi)/\text{diam}(\phi + \pi/2))$ where $\text{diam}(\phi)$ means the diameter of the particle in the ϕ -direction.

³ We provide in the appendix the main details of this result.

$f(\Sigma, H, n)$ obeying relations (10) and (11), linear with respect to Σ and affine with respect to H is given by

$$f = \bar{l}\Sigma n + \sum_{i=2}^6 \alpha_i I_i \tag{12}$$

where $\alpha_i \in \mathbb{R}$ and the vector-valued invariants $I_i(\Sigma, H, n)$ are given by

$$I_2 = 2\Sigma n + (\text{tr}\Sigma)n - 4(n \cdot \Sigma n)n \tag{13}$$

$$I_3 = (\text{tr}\Sigma)(\text{tr}H)n - 4(\text{tr}\Sigma)(n \cdot Hn)n + 8(n \cdot \Sigma n)Hn - 4H\Sigma n \tag{14}$$

$$I_4 = (\text{tr}\Sigma)(\text{tr}H)n - 4(\text{tr}H)(n \cdot \Sigma n)n + 8(n \cdot Hn)\Sigma n - 4\Sigma Hn \tag{15}$$

$$I_5 = (\text{tr}\Sigma)(\text{tr}H)n - 8(n \cdot Hn)(n \cdot \Sigma n)n + 2[H\Sigma n + \Sigma Hn] \tag{16}$$

$$I_6 = (\text{tr}\Sigma)(\text{tr}H)n - 16(n \cdot Hn)(n \cdot \Sigma n)n + 4[(\Sigma n \cdot Hn)n + (n \cdot Hn)\Sigma n + (n \cdot \Sigma n)Hn] \tag{17}$$

We note that using the above definitions one can easily check that the consistency condition is automatically verified since for any Σ, H , and $i = 2, \dots, 6$ we have

$$\int_0^{2\pi} \Sigma n \otimes n d\theta = \pi \Sigma, \quad \int_0^{2\pi} I_i \otimes n d\theta = 0.$$

For practical reasons related to the identification procedure, we remark that the first two terms in (12) provide relation (9) so that, we split (12) as

$$f(\Sigma, H, n) = g(\Sigma, n) + h(\Sigma, H, n). \tag{18}$$

where

$$g(\Sigma, n) = \bar{l}\Sigma n + \alpha_2 I_2(\Sigma, n), \tag{19}$$

$$h(\Sigma, H, n) = \sum_{i=3}^6 \alpha_i I_i(\Sigma, H, n). \tag{20}$$

As H is introduced to account for the structural anisotropy of the sample, and (12) is a generalization of (9), subsequently we call g the *isotropic part* and (\bar{l}, α_2) the isotropic parameters. Moreover, we call h the *anisotropic part* and $(\alpha_i)_{i=3, \dots, 6}$ the anisotropic parameters.

4 Numerical samples and branch tensor

4.1 Numerical samples description

The numerical tests we worked with, previously reported in [11], were performed on samples containing polygonal rigid particles and Coulomb friction. They involve two samples: a first one containing particles with aspect ratio 1

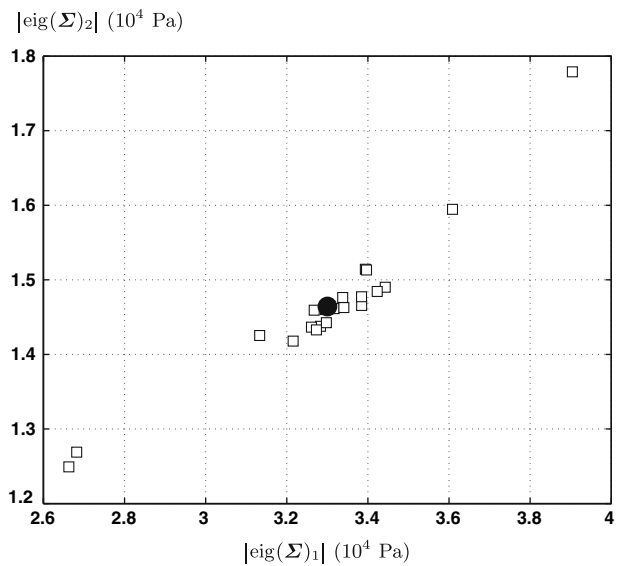


Fig. 1 Absolute values (white squares) of the principal stresses computed for 21 states around the macroscopic horizontal deformation 30% in the sample containing elongated particles. Numerical data show a significant dispersion ($\sim 30\%$) around the eigenvalues of the averaged stress (black circle) due to dry friction interactions between particles

and a second one containing elongated particles with aspect ratio 3. The tests are classical biaxial tests where the imposed deformation rate is $\dot{\epsilon} = 5 \times 10^{-2} \text{ s}^{-1}$ for the ratio 1 sample and $\dot{\epsilon} = 10^{-1} \text{ s}^{-1}$ for the ratio 3 sample. The time step for numerical integration in all cases is $\Delta t = 5 \times 10^{-5} \text{ s}$.

It is well-known that Coulomb friction at the microscale provides results with significant numerical noise which means that for two configurations at equilibrium very close to each other the fluctuations in the macroscopic stress may reach 30% as shown on Fig. 1. In order to filter such behavior we collect data from 21 configurations situated just before and just after a given state, at fixed time intervals $\Delta T = 100 \times \Delta t$. It follows that, for example, near a state where the horizontal deformation is 30% for the ratio 3 sample, we record contact forces, particles positions and contact positions from 29.95 up to 30.05%, each 0.005%. We choose as a representative for a horizontal deformation of 30% the configuration for which the macroscopic stress is closest to the average macroscopic stress of the 21 states described above.

The ratio 1 sample, denoted in the following by R1-sample, is a rectangular box (22 cm \times 16.5 cm) containing 4,789 polygonal particles with a diameter dispersion⁴ of 2.6. The deposit is realized under gravity, the initial volume fraction is 0.21 and the friction coefficient was fixed to

⁴ This dispersion is given on the basis of the diameter of the smallest disk containing a particle.

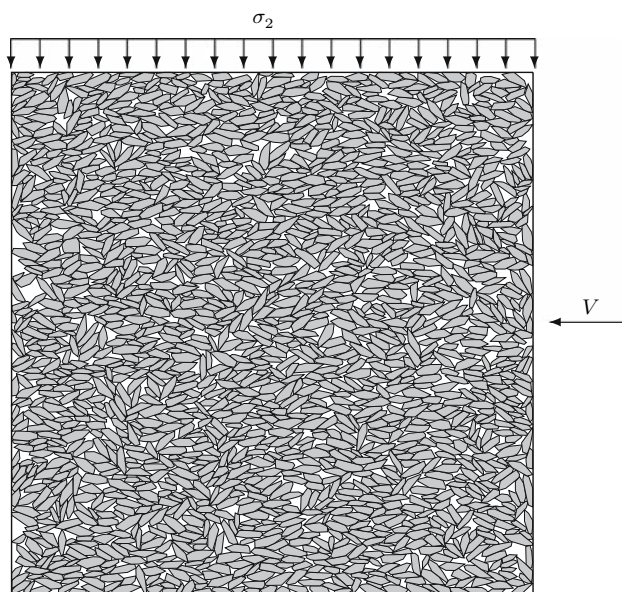


Fig. 2 Initial state for the aspect ratio 3 sample

0.3. Contact positions, positions of the particles centers and the contact forces were recorded at horizontal deformation corresponding to 5, 10, 20, and 30%, respectively, following the above mentioned procedure. Subsequently, these configurations will be denoted by $R1_5$, $R1_{10}$, $R1_{20}$, and $R1_{30}$.

The ratio 3 sample, or shortly R3-sample, is a rectangular box (11 cm × 11 cm) containing 1,937 polygonal particles with a diameter dispersion of 2.85. The deposit is realized under gravity so, as a consequence, the initial state is highly anisotropic. The initial volume fraction is 0.29 and the friction coefficient was fixed to 0.3. Contact positions, positions of the particles centers and the contact forces were recorded at horizontal deformation corresponding to 5, 10, 20, 30, 36 and 39%, respectively, and for convenience we shall denote these configurations by $R3_{10}$, $R3_{20}$, $R3_{30}$, $R3_{36}$ and $R3_{39}$.

An illustration of the sample in the initial state is presented in Fig. 2.

The values of the stress tensors⁵ for fixed deformations above are given in the Table 1. The biaxial tests realized on both samples give, for each configuration

- the set of normal and tangential components of the contact forces,
- the positions of each contact point and contact orientations,
- the positions of centers of mass for each particle.

These data are sorted and averaged as explained in Sect. 2.2. The numerical results to be fitted by the

⁵ For the rest of the paper, we shall use the classical convention in solid mechanics: a compression stress is negative.

Table 1 Values of the macroscopic stress (in Pa) computed using (7) for each sample

State	Σ	State	Σ
$R1_5$	$\begin{pmatrix} -20909 & 467 \\ 467 & -10668 \end{pmatrix}$	–	–
$R1_{10}$	$\begin{pmatrix} -25664 & -498 \\ -498 & -11441 \end{pmatrix}$	$R3_{10}$	$\begin{pmatrix} -23234 & -344 \\ -344 & -11382 \end{pmatrix}$
$R1_{20}$	$\begin{pmatrix} -29318 & -99 \\ -99 & -12248 \end{pmatrix}$	$R3_{20}$	$\begin{pmatrix} -27698 & 455 \\ 455 & -12832 \end{pmatrix}$
$R1_{30}$	$\begin{pmatrix} -32766 & -407 \\ -407 & -14031 \end{pmatrix}$	$R3_{30}$	$\begin{pmatrix} -33871 & -311 \\ -311 & -14854 \end{pmatrix}$
–	–	$R3_{36}$	$\begin{pmatrix} -39055 & -234 \\ -234 & -16781 \end{pmatrix}$
–	–	$R3_{39}$	$\begin{pmatrix} -39820 & -595 \\ -595 & -17816 \end{pmatrix}$

representation formula are the k values of the orientational averaged contact forces (f_n^{exp} , f_t^{exp}) obtained with an orientational resolution fixed here to $k = 36$.

4.2 Justification for the choice of $\mathbf{H} = \langle \mathbf{l} \otimes \mathbf{l} \rangle$

The motivation for a representation formula more complex than relation (9) is based on the following remark: for quite identical stress tensors values, the shape of the (f_n^{exp} , f_t^{exp}) data is quite different for the R1-sample and for the R3-sample as shown Fig. 3. The elongated particles of the R3-sample seem to influence in a significant way the numerical results shape. In order to improve the representation formula we choose to use an internal variable \mathbf{H} able to account for the aspect ratio. As noted in Sect. 2.2 the branch vector can do this, while the contact vector can not.

To support this remark, we represent in Fig. 4 all the considered configurations in the \mathbf{H} -eigenvalues plane. On this figure, each point is representative of a given configuration Ri_j and the so-called isotropic line is defined as the set of points corresponding to isotropic configurations:

\mathbf{H} reflects an isotropic configuration

$$\Leftrightarrow \mathbf{H} = \lambda \mathbf{I}_d, \lambda \in \mathbb{R}^* \tag{21}$$

The ability of \mathbf{H} to reflect the structural anisotropy of a granular sample is clearly emphasized on this figure: the range occupied by the representative points of the R3-sample is significantly larger than the one occupied by the representative points of the R1-sample. The physical evidence that the R3-sample may exhibit a real structural anisotropy (in the sense of (21)) much more important than the R1-sample is thus well reflected by this choice of the internal variable \mathbf{H} .

5 Identification procedure and results

In a previous work on modeling contact forces distribution in granular samples containing elongated particles [2], we adopt an identification procedure based on all the data for a given granular sample. The main drawback of this idea is the fact that it uses data for all configurations, so that its predictive character is missing. Accordingly, hereafter we present a different method which exhibits a predictive character.

In this work our goal is twofold:

- we propose a representation formula that cover a large class of shapes using an additional internal variable and,
- we want to insure a predictive character of the representation using a suitable identification procedure.

To this end, this section presents both the description of the identification procedure used to fit the numerical simulations results and the analysis of the isotropic and the anisotropic parameters contribution in the representation formula.

5.1 Quality index

Once the identification is performed, the theoretical orientational contact forces distribution, $f(\Sigma, H, n) = (f_n, f_t)$, has to be compared to the experimental data, $f^{exp} = (f_n^{exp}, f_t^{exp})$, as those presented on Fig. 3. To achieve this we define a quality index, denoted q , able to evaluate a relative distance between the theoretical distribution and the experimental data through

$$q = \frac{\|f(\Sigma, H, n) - f^{exp}\|}{\|f^{exp}\|} = \left[\frac{(f_n - f_n^{exp})^2 + (f_t - f_t^{exp})^2}{(f_n^{exp})^2 + (f_t^{exp})^2} \right]^{1/2} \tag{22}$$

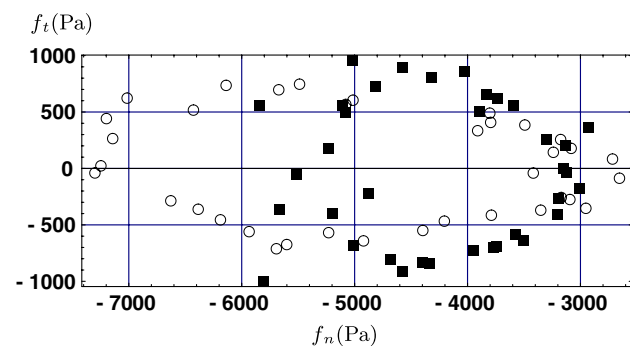


Fig. 3 Shapes of the (f_n^{exp}, f_t^{exp}) data corresponding to the configurations $R1_{10}$ (open circles) and $R3_{10}$ (filled squares) having stress tensors of the same order of magnitude

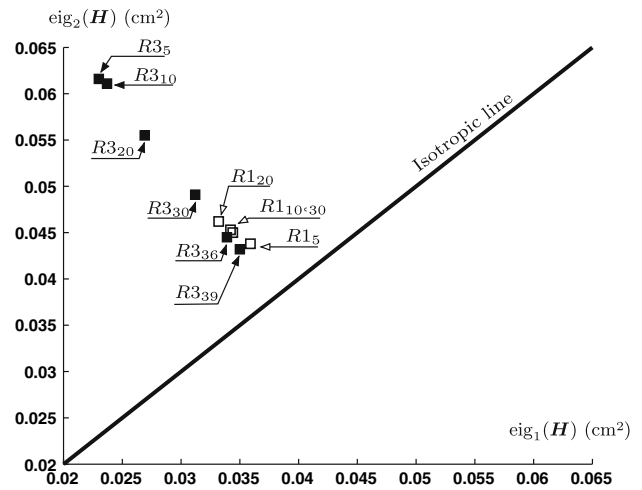


Fig. 4 Configurations of the $R1$ -sample and $R3$ -sample in the space of the H -eigenvalues to show the ability of H to represent the structural anisotropy. The most anisotropic states for the $R3$ -sample, $R3_5$ and $R3_{10}$, reflect the initial deposit under gravity, which for elongated particles produces anisotropic microstructures

In the following, the quality index will be used to estimate the improvement due to both isotropic and anisotropic parameters.

5.2 Identification procedure

5.2.1 Preliminary remarks on the meaning of \bar{d}

As mentioned in Sect. 2.2, previous studies [4, 8, 11], define \bar{d} in (8) as the *averaged particle diameter*, depending on the considered elongation ratio R_a , and defined as:

$$\bar{d} = \frac{1}{2} \left(1 + \frac{1}{R_a} \right) d^*, \tag{23}$$

where d^* is the diameter of the smallest disk centered at the particle’s mass center and containing all vertices of the polygonal particle. According to this definition, $\bar{d} = 0.36$ cm for the $R1$ -sample and $\bar{d} = 0.32$ cm for the $R3$ -sample. Considering \bar{d} as fixed for a given sample and using the formula (9) for the theoretical distribution, the only remaining parameter to be identified is $\alpha_2 = \bar{l}\mu$. A classical least squares method performed on the following quadratic objective function,

$$\delta(\Sigma, n) = (f_n(\Sigma, n) - f_n^{exp})^2 + (f_t(\Sigma, n) - f_t^{exp})^2, \tag{24}$$

returns quality index values near $q = 74\%$! This result shows that \bar{d} can not be defined as the averaged particles diameter. We have to note that \bar{d} appears in the continuum limit of (7) when the term $\langle l_{ij} \rangle_a$ is written as

$$\langle \mathbf{I}_{ij} \rangle_a = d(\theta_a) \mathbf{n}(\theta_a) \quad (25)$$

and all we can expect⁶ is \bar{d} less than mean diameter. Instead of fixing \bar{d} to the averaged particles diameter we choose to consider \bar{l} defined through:

$$\frac{N\pi\bar{d}}{|\mathcal{P}|} = \frac{1}{\bar{l}} \quad (26)$$

as a parameter to be identified, as well as α_2 . This point of view leads to significant improvement of the quality index values as shown in what follows.

5.2.2 Description of the identification procedure

As the internal variable \mathbf{H} has been introduced to account for the structural anisotropy of the samples, we propose to identify the set of isotropic parameters (\bar{l}, α_2) on the most isotropic configuration and the set of anisotropic parameters $(\alpha_i)_{i=3,\dots,6}$ on the most anisotropic configuration. The above remark leads to the following identification procedure:

Step 1: Definition of a criterion able to find the most isotropic configuration and the most anisotropic one among the set of all the configurations for a given sample. For this, we use the representation of the different configurations in the H -eigenvalues plane, as in Fig. 4. Indeed, by definition (21), the distance from a representative point to the isotropic line measures the anisotropy of the associated configuration. It can thus be concluded that, according to the chosen internal variable, $R1_5$ and $R1_{20}$ are the most isotropic and the most anisotropic configurations of the R1-sample, respectively. Likewise, $R3_{39}$ and $R3_{10}$ ⁷ are the most isotropic and the most anisotropic configurations of the R3-sample, respectively.

Step 2: Identification of the two isotropic parameters (\bar{l}, α_2) . Denoting by $\boldsymbol{\Sigma}^{\text{iso}}$ the stress tensor associated to the most isotropic configuration, the objective function is:

$$\delta(\bar{l}, \alpha_2) = (g_n(\boldsymbol{\Sigma}^{\text{iso}}, \mathbf{n}) - f_n^{\text{exp}})^2 + (g_t(\boldsymbol{\Sigma}^{\text{iso}}, \mathbf{n}) - f_t^{\text{exp}})^2. \quad (27)$$

As the objective function is quadratic the least squares method returns a unique set of isotropic parameters subsequently denoted by $(\bar{l}^{\text{iso}}, \alpha_2^{\text{iso}})$ such that the isotropic part of the identified distribution is for all stress tensor $\boldsymbol{\Sigma}$ and for all unit vector \mathbf{n} :

⁶ In the continuum limit d is dependent of θ but the first term of its Fourier series is what we denote here \bar{d} .

⁷ Actually, Fig. 4 exhibits $R3_5$ to be the most anisotropic configuration; this configuration will nevertheless not be used in the following because it is the only configuration that corresponds to the dilatancy phase of the material behavior.

$$\mathbf{g}^{\text{iso}}(\boldsymbol{\Sigma}, \mathbf{n}) = \bar{l}^{\text{iso}} \boldsymbol{\Sigma} \mathbf{n} + \alpha_2^{\text{iso}} \mathbf{I}_2. \quad (28)$$

When the searched distribution looks like formula (9) these parameters are sufficient to predict the distribution for the configurations $(R1_{10}, R1_{20}, R1_{30})$ and $(R3_{10}, R3_{20}, R3_{30}, R3_{36})$ respectively, using

$$\mathbf{f}(\boldsymbol{\Sigma}, \mathbf{n}) = \mathbf{g}^{\text{iso}}(\boldsymbol{\Sigma}, \mathbf{n}).$$

Step 3: Identification of the four parameters $(\alpha_i)_{i=3,\dots,6}$ describing the anisotropic part using the most anisotropic configuration for each sample. Denoting by $\boldsymbol{\Sigma}^{\text{an}}$ and \mathbf{H}^{an} the stress tensor and the texture tensor associated to the most anisotropic configuration, respectively, the objective function is:

$$\begin{aligned} \delta(\alpha_3, \alpha_4, \alpha_5, \alpha_6) = & (g_n^{\text{iso}}(\boldsymbol{\Sigma}^{\text{an}}, \mathbf{n}) + h_n(\boldsymbol{\Sigma}^{\text{an}}, \mathbf{H}^{\text{an}}, \mathbf{n}) - f_n^{\text{exp}})^2 \\ & + (g_t^{\text{iso}}(\boldsymbol{\Sigma}^{\text{an}}, \mathbf{n}) + h_t(\boldsymbol{\Sigma}^{\text{an}}, \mathbf{H}^{\text{an}}, \mathbf{n}) - f_t^{\text{exp}})^2. \end{aligned} \quad (29)$$

Once again, as the objective function is quadratic the least squares method returns a unique solution set for the identified anisotropic parameters denoted by $(\alpha_i^{\text{an}})_{i=3,\dots,6}$ such that the anisotropic identified part of the distribution is:

$$\mathbf{h}^{\text{an}}(\boldsymbol{\Sigma}, \mathbf{H}, \mathbf{n}) = \sum_{i=3}^6 \alpha_i^{\text{an}} \mathbf{I}_i. \quad (30)$$

Finally

$$\mathbf{f}(\boldsymbol{\Sigma}, \mathbf{H}, \mathbf{n}) = \mathbf{g}^{\text{iso}}(\boldsymbol{\Sigma}, \mathbf{n}) + \mathbf{h}^{\text{an}}(\boldsymbol{\Sigma}, \mathbf{H}, \mathbf{n}). \quad (31)$$

will be used to predict the distribution for all configurations, even if not used in the identification procedure.

5.3 Results and interpretations

5.3.1 Identification results

Following the above discussed identification procedure, we found the isotropic and anisotropic parameters listed in Table 2. To discuss the approximation level we summarize the quality indexes for different cases in Tables 3 and 4. In both tables:

- (1) The line **PrIso** represents the quality indexes, q_{PrIso} , of the so-called **Predicted** distributions using only the **I**sotropic parameters. It means that, whatever the considered configuration characterized by a stress tensor $\boldsymbol{\Sigma}$, the quality indexes are computed using only the isotropic part of the distribution, $\mathbf{g}^{\text{iso}}(\boldsymbol{\Sigma}, \mathbf{n})$, with the isotropic parameters, \bar{l}^{iso} and α_2^{iso} , identified on $R1_5$ and $R3_{39}$ for the R1-sample and the R3-sample, respectively.

Table 2 Values of the identified parameters of the theoretical distribution

	R1-sample	R3-sample
\bar{l}^{iso} (cm)	0.263	0.247
α_2^{iso} (cm)	-0.058	-0.031
α_3^{an} (cm ⁻¹)	1.565	0.165
α_4^{an} (cm ⁻¹)	-0.224	-0.049
α_5^{an} (cm ⁻¹)	1.507	-0.086
α_6^{an} (cm ⁻¹)	-0.625	0.145

The most isotropic configuration and the most anisotropic one were defined using the distance to the isotropic line as explained in Step 1 of the identification procedure

Table 3 Quality indexes for the identified and predicted distributions of the R1-sample

	R1 ₅	R1 ₁₀	R1 ₂₀	R1 ₃₀
PrIso (%)	7.95	12.26	15.92	15
PrAn (%)	7.90	11.84	15.17	14.66
BAn (%)	7.57	10.95	14.41	13.85
Gap₁ (%)	5.02	11.96	10.48	8.30
Gap₂ (%)	4.36	8.13	5.27	5.83

Table 4 Quality indexes for the identified and predicted distributions of the R3-sample

	R3 ₁₀	R3 ₂₀	R3 ₃₀	R3 ₃₆	R3 ₃₉
PrIso (%)	13.46	14.80	13.41	13.27	11.08
PrAn (%)	12.52	14.16	13.12	13.24	11.31
BAn (%)	11.76	13.30	12.40	12.70	10.80
Gap₁ (%)	14.46	11.28	8.40	4.49	2.59
Gap₂ (%)	6.46	6.47	5.81	4.25	4.72

(2) Likewise, the line **PrAn** represents the quality indexes, q_{PrAn} , of the so-called **Predicted** distributions using simultaneously the isotropic and the **Anisotropic** parameters. This means that, whatever the considered configuration characterized by a stress tensor Σ and an internal variable H , the quality indexes are computed using the distribution

$$g^{\text{iso}}(\Sigma, n) + h^{\text{an}}(\Sigma, H, n),$$

with the isotropic parameters, \bar{l}^{iso} and α_2^{iso} , identified as above, and with additional anisotropic parameters $(\alpha_i^{\text{an}})_{i=3, \dots, 6}$ identified on R1₂₀ for the R1-sample and on R3₁₀ for the R3-sample, respectively. This line contains the result of the identification procedure proposed in Sect. 5.2.

(3) The line **BAn** represents the quality indexes of the so-called **Best** distributions using simultaneously the isotropic and the **Anisotropic** parameters. This means

that both the isotropic and the anisotropic parameters are identified on each configuration. This leads to the best quality index, q_{BAn} , that can ever be obtained according to the least squares method.

(4) The line **Gap₁** represents the relative gap between the quality indexes of the predicted distribution **PrIso** and the best distribution **BAn**:

$$\text{Gap}_1 = \frac{q_{\text{PrIso}} - q_{\text{BAn}}}{q_{\text{BAn}}}. \quad (32)$$

(5) The line **Gap₂** represents the relative gap between the quality indexes of the predicted distribution **PrAn** and the best distribution **BAn**:

$$\text{Gap}_2 = \frac{q_{\text{PrAn}} - q_{\text{BAn}}}{q_{\text{BAn}}}. \quad (33)$$

5.3.2 Meaning of \bar{d}

The numerical values of \bar{l}^{iso} in Tables 3 and 4 lead, according to relation (23), to the following values for \bar{d} :

$$\begin{cases} \bar{d} = 0.092 \text{ cm} & \text{for the R1-sample,} \\ \bar{d} = 0.080 \text{ cm} & \text{for the R3-sample.} \end{cases} \quad (34)$$

As noted at the beginning of Sect. 5.2, using the averaged diameter for \bar{d} overestimates the normal and tangential components of the averaged contact forces and moreover provides a poor quality index whose order of magnitude is 74%. Alternatively, when we identify \bar{l} and subsequently calculate the corresponding \bar{d} we find a value quarter of the averaged particles diameter. The correct interpretation of this result relies on the use of the average in relation (26) which, as noted after (25) is lower than the average diameter of particles due to orientational dispersion of the branch vectors.

5.3.3 Predictive character of the identification procedure

The best distribution is used as a measure to quantify the predictive character of our identification procedure via the **Gap** indexes. As Tables 3 and 4 show clearly the predicted distributions lead always to quality indexes that are very closed to the ones of the best distributions.

5.3.4 Improvement due to the use of the internal variable H

The first non trivial result concerning the internal variable H and the proposed identification procedure is the following stability property: we found that the identification

of $f(\Sigma, H, n)$ generally exhibits better quality indexes than the identification of $f(\Sigma, n)$. This is not obvious a priori since improving the quality of a given configuration using the anisotropic part of the representation formula could have increased the error for other configurations.

It should be noted that the reference for any comparison are the quality indexes obtained with the best distributions. Indeed, these distributions allow to quantify the improvement due to the use of the internal variable H . As shown in Figs. 5 and 6 the improvement due to the use of the internal variable H can reach 50% for the most anisotropic configurations. In fact, more anisotropic configuration, higher improvement. Likewise, more isotropic configuration, nearest the quality indexes q_{PrIso} , q_{PrAn} , and q_{BAAn} . Moreover, by comparison between numerical values of \mathbf{Gap}_1 and \mathbf{Gap}_2 in Tables 3 and 4 one may note that using the anisotropic part in the representation formula not only improves the overall quality for (almost) all configurations considered, but also gives a more uniform relative distance between the predicted distribution and the best one. This is the consequence of the identification procedure based on most isotropic and most anisotropic configurations.

A natural question concerns the quality indexes q_{BAAn} which, as shown in Tables 3 and 4, are not better than 7.57 and 10.80% for the $R1$ -sample and the $R3$ -sample, respectively. This probably relies on the fact that the normal and the tangential components of contact forces are not of the same order of magnitude while they have to be fitted both by the same representation formula. The best quality obtained is probably limited by the norm of the difference between the two components; this point should be investigated further. A possible solution to overcome the differences in the orders of magnitude is to put a suitable weight on the tangential component in order to obtain

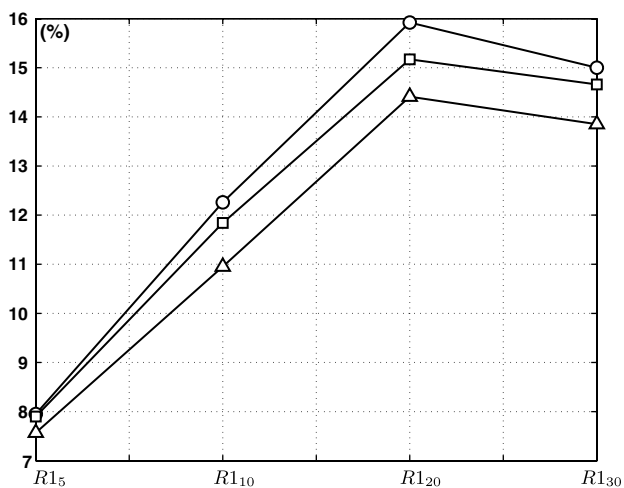


Fig. 5 Evolution of the quality indexes during the deformation process of the $R1$ -sample: q_{PrIso} (line with circles), q_{PrAn} (line with squares), q_{BAAn} (line with triangles)

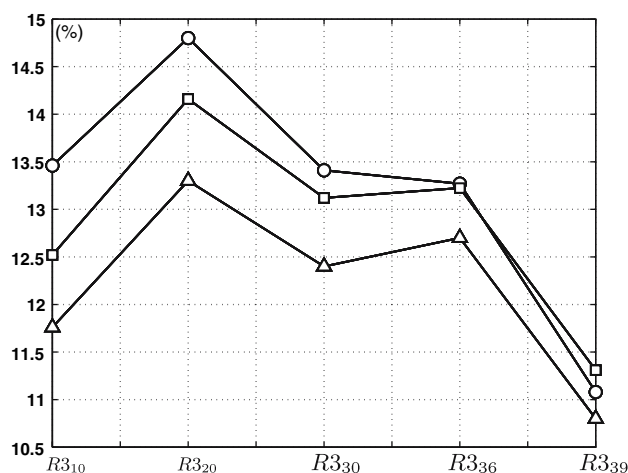


Fig. 6 Evolution of the quality indexes during the deformation process of the $R3$ -sample: q_{PrIso} (line with circles), q_{PrAn} (line with squares), q_{BAAn} (line with triangles)

normalized orders of magnitude for both normal and tangential components, but a choice of a physically meaningful weight is still an open problem. Related to this, we underline the choice of the graphical representation for the distributions: while Figs. 7 and 8 are easy to interpret in terms of quality of the distributions, one must be more careful when interpreting Fig. 9 which represents the same data, from $R3_{10}$ sample. All these pictures represent theoretical f and experimental values (both weighted by $p(\theta)$) of normal and tangential contact forces distributions in different configurations. Visually, in Fig. 9 the continuous line seems closer to the numerical values (points) than the dashed line. However, by inspection in Table 4 the quality index of the latter is better than the quality index of the former.

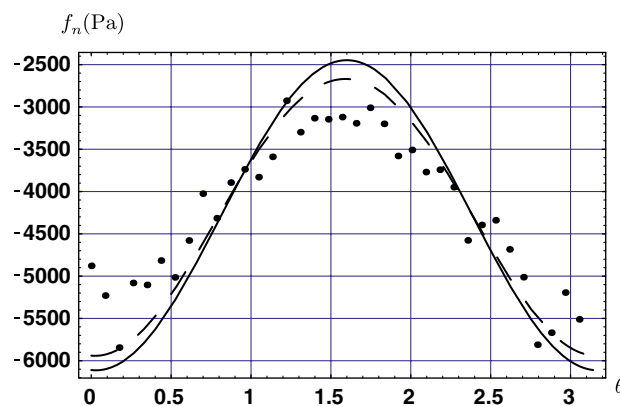


Fig. 7 Theoretical and experimental normal contact forces distributions for the configuration $R3_{10}$ with respect to θ , the orientation of the unit normal vector at the contact. The points represent the experimental data, the continuous line represents the theoretical distribution g_n^{iso} , and the dashed line represents the theoretical distribution $g_n^{iso} + h_n^{an}$. The distribution involving all the parameters seems better than the one involving just the isotropic parameters

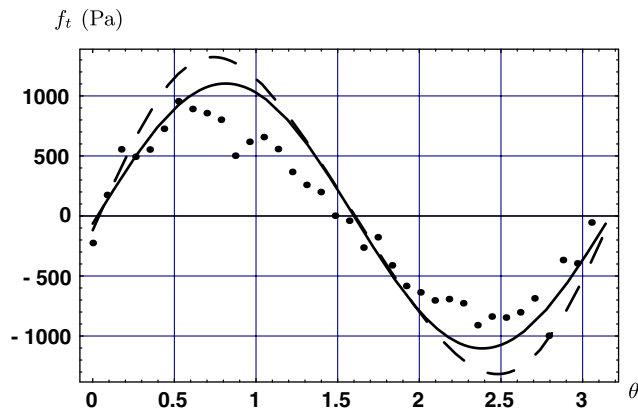


Fig. 8 Theoretical and experimental tangential contact forces distributions for the configuration $R3_{10}$ with respect to θ . The points represent the experimental data, the *continuous line* represents the theoretical distribution g_t^{iso} , and the *dashed line* represents the theoretical distribution $g_t^{iso} + h_t^{an}$. The distribution involving all the parameters seems worse than the one involving just the isotropic parameters. It should be noted that the quality of a given analytic relation is defined in (22) in terms of both approximations of normal and tangential components, which cannot be dissociated

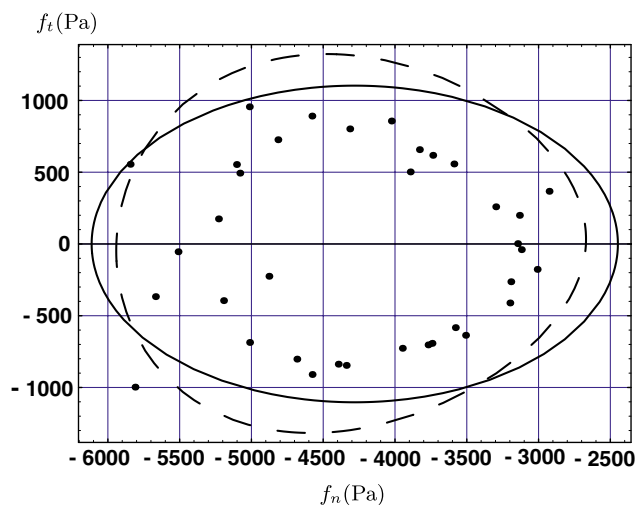


Fig. 9 Shapes of the theoretical distributions for the configuration $R3_{10}$: numerical simulation results (f_n^{exp}, f_t^{exp}) (points), (g_n^{iso}, g_t^{iso}) (continuous line), and $(g_n^{iso} + h_n^{an}, g_t^{iso} + h_t^{an})$ (dashed line). The latter theoretical distribution exhibits better quality index than the former

6 Conclusions and open questions

In this paper, we investigate the role of the branch tensor $\mathbf{H} = \langle \mathbf{I} \otimes \mathbf{I} \rangle$ as a possible candidate for an internal variable able to account for the anisotropic character of the microstructure in a granular sample containing elongated particles. The branch tensor is a natural candidate because: (i) it contains nonlocal information about the relative positions between particles; (ii) it is used in the homogenization operator (Weber relation) and (iii) it is included in

the localization operator in some simple cases (classical discrete homogenization) when explicit localization formulae are available.

Introduction of a supplemental internal variable in the localization operator leads to a more complex formula for localization operator and the need for a new identification procedure. We propose an identification procedure which dissociate the isotropic and the anisotropic parts of the localization operator. The continuum limit of the discrete Weber relation (after rearrangement) introduces naturally a characteristic length, above denoted \bar{l} , and previously related to the averaged particles diameter. We choose to regard the characteristic length as a supplemental material parameter associated to the isotropic part. This point of view and the proposed identification procedure lead to a localization formula having the following properties:

- It gives a *predictive result for the localization operator*, i.e., based on two states along the deformation process the procedure is able to accurately predict for a given macroscopic stress and granular texture \mathbf{H} the orientational distribution of contact forces.
- It improves the isotropic localization operator *for all states along the deformation process*, including the anisotropic part identified on the most anisotropic state.
- *It improves drastically, from 74 to 15%*, the quality of the localization operator using \bar{l} as a material parameter.

Despite a constant improvement of the quality of the localization operator, which as expected, is more significant for strong anisotropic states, the overall improvement is penalized by the different orders of magnitude between the normal and tangential components of the contact forces.

Acknowledgments We kindly acknowledge detailed numerical results for biaxial tests, provided to us by Cécile Nougier and previously published in [11].

Appendix. Technical details of the result in (12)

This result is obtained in three steps using a classical representation result for isotropic functions due to Wang [15].

(a) General form for f

Using the general result in [15] we find that the general form of an isotropic function is a linear combination of vector-valued invariants below

$$\mathbf{n}, \quad \Sigma \mathbf{n}, \quad \mathbf{H} \mathbf{n}, \quad \Sigma \mathbf{H} \mathbf{n}, \quad \mathbf{H} \Sigma \mathbf{n}, \quad \Sigma^2 \mathbf{n}, \quad \mathbf{H}^2 \mathbf{n} \quad (35)$$

with coefficients depending on the following combinations

$$\begin{aligned} & \text{tr}(\mathbf{H}), \mathbf{n} \cdot \boldsymbol{\Sigma} \mathbf{n}, \mathbf{n} \cdot \mathbf{H} \mathbf{n}, \text{tr}(\boldsymbol{\Sigma}), \text{tr}(\mathbf{H} \boldsymbol{\Sigma}), \boldsymbol{\Sigma} \mathbf{n} \cdot \mathbf{H} \mathbf{n} \\ & \text{tr}(\boldsymbol{\Sigma}^2), \text{tr}(\boldsymbol{\Sigma}^3), \text{tr}(\mathbf{H}^2), \text{tr}(\mathbf{H}^3), \text{tr}(\mathbf{H}^2 \boldsymbol{\Sigma}), \\ & \text{tr}(\mathbf{H} \boldsymbol{\Sigma}^2), \text{tr}(\mathbf{H}^2 \boldsymbol{\Sigma}^2), \mathbf{n} \cdot \boldsymbol{\Sigma}^2 \mathbf{n}, \mathbf{n} \cdot \mathbf{H}^2 \mathbf{n}. \end{aligned} \tag{36}$$

By inspection in (36) only the first line contains terms at most linear in $\boldsymbol{\Sigma}$ and \mathbf{H} . Moreover, products between scalar-valued and vector-valued invariants lead to a general form for \mathbf{f} as

$$\mathbf{f}(\boldsymbol{\Sigma}, \mathbf{H}, \mathbf{n}) = \sum_{i=1}^{19} a_i \mathbf{f}_i(\boldsymbol{\Sigma}, \mathbf{H}, \mathbf{n}) \tag{37}$$

where $a_i \in \mathbb{R}$ and the list of vector-valued invariants \mathbf{f}_i is given by:

$$\begin{aligned} \mathbf{f}_1 &= \mathbf{n}, & \mathbf{f}_{10} &= \mathbf{H} \mathbf{n}, \\ \mathbf{f}_2 &= \text{tr}(\boldsymbol{\Sigma}) \mathbf{n}, & \mathbf{f}_{11} &= \text{tr}(\boldsymbol{\Sigma}) \mathbf{H} \mathbf{n}, \\ \mathbf{f}_3 &= \text{tr}(\boldsymbol{\Sigma}) \text{tr}(\mathbf{H}) \mathbf{n}, & \mathbf{f}_{12} &= (\mathbf{n} \cdot \boldsymbol{\Sigma} \mathbf{n}) \mathbf{H} \mathbf{n}, \\ \mathbf{f}_4 &= \text{tr}(\boldsymbol{\Sigma}) (\mathbf{n} \cdot \mathbf{H} \mathbf{n}) \mathbf{n}, & \mathbf{f}_{13} &= \boldsymbol{\Sigma} \mathbf{n}, \\ \mathbf{f}_5 &= (\mathbf{n} \cdot \boldsymbol{\Sigma} \mathbf{n}) \mathbf{n}, & \mathbf{f}_{14} &= \text{tr}(\mathbf{H}) \boldsymbol{\Sigma} \mathbf{n}, \\ \mathbf{f}_6 &= \text{tr}(\mathbf{H}) (\mathbf{n} \cdot \boldsymbol{\Sigma} \mathbf{n}) \mathbf{n}, & \mathbf{f}_{15} &= (\mathbf{n} \cdot \mathbf{H} \mathbf{n}) \boldsymbol{\Sigma} \mathbf{n}, \\ \mathbf{f}_7 &= (\mathbf{n} \cdot \boldsymbol{\Sigma} \mathbf{n}) (\mathbf{n} \cdot \mathbf{H} \mathbf{n}) \mathbf{n}, & \mathbf{f}_{16} &= \boldsymbol{\Sigma} \mathbf{H} \mathbf{n}, \\ \mathbf{f}_8 &= \text{tr}(\boldsymbol{\Sigma} \mathbf{H}) \mathbf{n}, & \mathbf{f}_{17} &= \mathbf{H} \boldsymbol{\Sigma} \mathbf{n}, \\ \mathbf{f}_9 &= (\mathbf{H} \mathbf{n} \cdot \boldsymbol{\Sigma} \mathbf{n}) \mathbf{n}, & \mathbf{f}_{18} &= \text{tr}(\mathbf{H}) \mathbf{n}, \\ & & \mathbf{f}_{19} &= (\mathbf{H} \mathbf{n} \cdot \mathbf{n}) \mathbf{n}. \end{aligned} \tag{38}$$

(b) Restrictions due to consistency relation

In (37) the a_i are restricted by the consistency condition (8); identification for symmetric part gives

$$\begin{aligned} a_1 &= 0, \\ a_5 &= -4a_2 \\ a_9 &= -4a_8 - \frac{1}{2}a_7 - a_6 - a_4 - 4a_3, \\ a_{12} &= -4a_{11} - \frac{1}{2}a_7 - a_6 - 3a_4 - 4a_3, \\ a_{13} &= 1 + 2a_2, \\ a_{15} &= -4a_{14} - 4a_3 - a_4 - 3a_6 - \frac{1}{2}a_7, \\ a_{17} &= -a_{16} + 2a_{14} + 2a_{11} + 2a_8 + \frac{1}{2}a_7 \\ & \quad + 3a_6 + 3a_4 + 8a_3, \\ a_{18} &= \frac{1}{2}a_{10}, \\ a_{19} &= -2a_{10}. \end{aligned} \tag{39}$$

and identification of the skew-symmetric part leads to

$$a_{16} = 2a_{14} + a_8 + \frac{1}{4}a_7 + 2a_6 + a_4 + 4a_3. \tag{40}$$

We shall denote by \mathbf{g}_i the factors in \mathbf{f} of a_i . Relations (39) and (40) reduce the number of coefficients a_i to nine, for $i \in I = \{2,3,4,6,7,8,10,11,14\}$.

(c) Linear independence of remaining invariants

Using \mathbf{g}_i we are lead to

$$\mathbf{f} = \boldsymbol{\Sigma} \mathbf{n} + \sum_{i \in I} a_i \mathbf{g}_i. \tag{41}$$

The following results are straightforward

- If

$$a_2 \mathbf{g}_2 + a_3 \mathbf{g}_3 + a_4 \mathbf{g}_4 + a_6 \mathbf{g}_6 + a_7 \mathbf{g}_7 + a_{10} \mathbf{g}_{10} = \mathbf{0}$$

for any $\boldsymbol{\Sigma}$ and any \mathbf{H} then $a_2 = a_3 = a_4 = a_6 = a_7 = a_{10} = 0$.

- We have for any $\boldsymbol{\Sigma}$ and \mathbf{H} :

$$-\mathbf{g}_3 + \mathbf{g}_4 + \mathbf{g}_6 + \mathbf{g}_8 = \mathbf{0}, \quad \mathbf{g}_4 = \mathbf{g}_{11}, \quad \mathbf{g}_6 = \mathbf{g}_{14}.$$

- One can easily check that

$$\mathbf{I}_2 := \mathbf{g}_2 = 2\boldsymbol{\Sigma} \mathbf{n} + (\text{tr} \boldsymbol{\Sigma}) \mathbf{n} - 4(\mathbf{n} \cdot (\boldsymbol{\Sigma} \mathbf{n})) \mathbf{n},$$

and

$$\mathbf{g}_{10} = 2\mathbf{H} \mathbf{n} + (\text{tr} \mathbf{H}) \mathbf{n} - 4(\mathbf{n} \cdot (\mathbf{H} \mathbf{n})) \mathbf{n},$$

while the four remaining invariants can be combined to give

$$\mathbf{I}_3 := \mathbf{g}_3 - 4\mathbf{g}_4, \quad \mathbf{I}_4 := \mathbf{g}_3 - 4\mathbf{g}_6,$$

$$\mathbf{I}_5 := \mathbf{g}_3 - 8\mathbf{g}_7, \quad \mathbf{I}_6 := \mathbf{g}_3 - 16\mathbf{g}_8,$$

thus leading finally to (12)–(17).

References

1. Cambou B, Jean M (2001) Micromécanique des matériaux granulaires, Hermes Science
2. Cambou B, Magoariéc H, Nouguiér C (2006) Influence of the particle shape on the distribution of contact forces in granular materials, communication at 6 th European Solid Mechanics Conference (ESMC-2006), Budapest (2006)
3. Chang CS, Hicher PY (2005) An elasto-plastic model for granular materials with microstructural consideration. Int J Solids Struct 42:4258–4277
4. Dedecker F (1999) Changements d'échelle dans les milieux granulaires à interactions complexes, Ph.D. thesis, Ecole Centrale de Lyon
5. Delyon F, Dufresne D, Lévy YE (1990) Physique et génie civil: deux illustrations simples. Ann des Ponts et Chaussées 53–54:22–29
6. Krut NP (2003) Contact forces in anisotropic frictional granular materials. Int J Solids Struct 40:3537–3556
7. Li XS, Dafalias YF (2002) Constitutive modelling of inherently anisotropic sand behaviour. J Geotech Environ Eng 128:868–880

8. Mahboubi A (1995) Contribution à l'étude micromécanique du comportement des matériaux granulaires par homogénéisation et approche numérique, Ph.D. thesis, Ecole Centrale de Lyon
9. Mehrabadi MM, Nemat-Nasser S, Oda M (1982) On statistical description of stress and fabric in granular materials. *Int J Numer Anal Methods Geomech* 6:95–108
10. Nemat-Nasser S, Zhang J (2002) Constitutive relations for cohesionless frictional material. *Int J Plast* 18:531–547
11. Noguier-Lehon C, Vincens E, Cambou B (2005) Structural changes in granular materials: the case of irregular polygonal particles. *Int J Solids Struct* 42:6356–6375
12. Oda M, Nemat-Nasser S, Mehrabadi MM (1982) A statistical study of fabric in a random assembly of spherical granules. *Int J Numer Anal Methods Geomech* 6:77–94
13. Sidoroff F, Cambou B, Mahboubi A (1993) Contact forces in granular media. *Mech Mater* 16:83–89
14. Tollenaere H, Caillerie D (1998) Continuous modeling of lattice structures by homogenization. *Adv Eng Softw* 29:699–705
15. Wang CC (1970) A new representation theorem for isotropic functions: An answer to Prof GF Smith criticism of my papers on representations for isotropic functions. *Arch Ration Mech Anal* 36:166–223